In-beam γ-ray spectroscopy of $^{37-42}$P

A. M. Hill,[1,2] A. Gade,[1,2] D. Bazin,[1,2] B. A. Brown,[1,2] B. Elman,[1,2] P. Farris,[1,2] J. Li,[1]
B. Longfellow,[1,2,*] J. Pereira,[1] A. Revel,[1] D. Rhodes,[1,2] M. Spieker,[1,†] and D. Weisshaar[1]

[1]*National Superconducting Cyclotron Laboratory, Michigan State University, East Lansing, Michigan 48824, USA*
[2]*Department of Physics and Astronomy, Michigan State University, East Lansing, Michigan 48824, USA*

(Dated: May 24, 2021)

The level schemes of the neutron-rich $^{37-42}$P isotopes are investigated via in-beam γ-ray spectroscopy following the fragmentation of a ^{45}Cl projectile beam at intermediate beam energies. Information on $\gamma\gamma$ coincidence relationships complemented by comparisons to shell-model calculations in the *sd-pf* model space were used to construct excitation level schemes for these neutron-rich nuclei. For the odd-mass ^{37,39}P isotopes, a level scheme is presented that appears essentially complete at low energies and exhausts the states predicted by the SDPF-MU shell-model Hamiltonian. Simple Nilsson configurations are proposed for the low-lying excited states of ^{38,39,40,41}P from an analysis of the $E2$ transition matrix elements and moments calculated within the shell model.

I. INTRODUCTION

Just below the neutron-rich Ca isotopic chain, the even-Z Si, S, and Ar isotopes beyond neutron number $N = 20$ have revealed rapid structural changes manifested in both the evolution of the single-particle structure as well as the collective degrees of freedom [1–3]. In fact, the breakdown of $N = 28$ magic number has been demonstrated in ^{42}Si and ^{44}S from the low-lying level schemes and the electromagnetic transition strengths [4–7]. Such discoveries of shell evolution continue to fuel intense experimental and theoretical efforts worldwide to understand the nuclear structure at the fringes of the nuclear chart. Over the past years, systematic studies along these even-Z isotopic chains leading up to and crossing $N = 28$ [8–15] have served to benchmark nuclear models that aim to describe this shell evolution in the neutron-rich regime on a quest for predictive power [2, 16]. The properties of S and Si isotopes are well described by shell-model calculations with the SDPF-MU effective interaction which was optimized to model the shape transition in the sulfur isotopic chain near $N = 28$ [17, 18] (see, for example, [12, 14, 18–20]).

The odd-Z isotopes located in between Si, S, and Ar on the nuclear chart have received less attention as their spectroscopy and level structure are more complex. While the systematics of the excitation spectra for $Z = 17$ Cl were explored in Ref. [21], there had been no such systematic effort for $Z = 15$ along the P isotopic chain. The phosphorus isotopes are of interest as they are located in between the S and Si isotopes, both of which show evidence for a rapid onset of collectivity and shape as well as configuration coexistence towards $N = 28$ [19, 20, 22–25]. Several phosphorus isotopes in this region have been studied previously in a variety of different experiments [6, 22, 26–32], but their level schemes remained elusive, even at low excitation energies.

Here, we report on the in-beam γ-ray spectroscopy study of $^{37-42}$P produced in the fragmentation of an intermediate-energy ^{45}Cl projectile beam on a C target. Level schemes, lifetimes of longer-lived excited states (in the few hundred picoseconds to nanosecond range), and associated transition strengths are presented and compared to shell-model calculations based on the SDPF-MU Hamiltonian.

II. EXPERIMENT

The measurements were performed at the Coupled Cyclotron Facility at the National Superconducting Cyclotron Laboratory [33] on the campus of Michigan State University. The ^{45}Cl projectiles were produced from a 140 MeV/u ^{48}Ca primary beam impinging upon a 1034 mg/cm^2 ^{9}Be production target and separated with a 750 mg/cm^2 Al degrader in the A1900 fragment separator [34]. The total momentum acceptance of the A1900 was limited to $\Delta p/p = 1.08\%$. The secondary projectile beam interacted with a 149 mg/cm^2 pyrolytic ^{12}C reaction target placed at the pivot point of the S800 spectrograph [35], with a mid-target energy of 62.5 MeV/u. The projectile-like reaction residues emerging from the target were identified event-by-event with the focal-plane detection system of the spectrograph [36] and time-of-flight information taken between plastic scintillators in the beam line upstream of the reaction target and in the back of the S800 focal plane. Two different settings of the S800 magnetic rigidity allowed $^{37-40}$P and $^{40-42}$P, respectively, to enter the focal plane. The particle identification spectra correlating the energy loss of the reaction residues measured in the S800 ionization chamber and their time of flight are shown in Fig. 1; for both settings, the various P isotopes can be unambiguously separated.

The ^{12}C reaction target was surrounded by the Gamma Ray Energy Tracking In-beam Nuclear Array

*Present Address: Lawrence Livermore National Laboratory, 7000 East Ave., Livermore, CA 94550, USA
†Present Address: Department of Physics, Florida State University, Tallahassee, FL 32306, USA

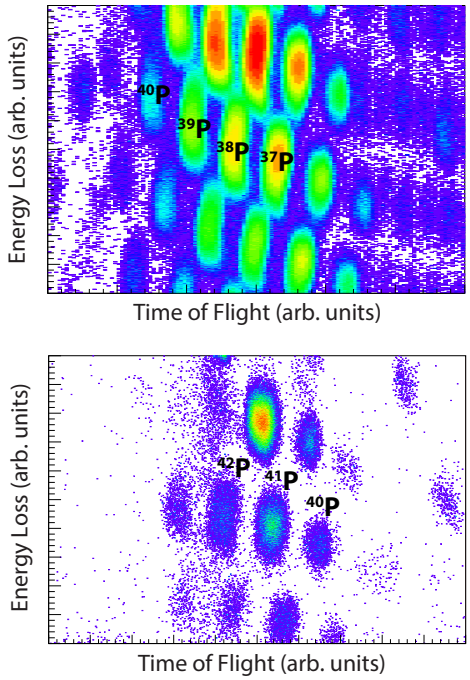

FIG. 1: Particle identification spectra for the reaction residues produced in ^{12}C(^{45}Cl,X+γ)Y with the magnetic rigidity of the S800 spectrograph centered on ^{46}Ar (upper panel) and ^{45}S (lower panel). The energy loss was measured with the ionization chamber of the S800 focal plane. The time-of-flight was taken between plastic scintillators in the beam line upstream of the target and in the back of the S800 focal plane (in the plots, the time of flight increases from right to left). The P isotopes of interest are unambiguously identified and separated.

(GRETINA) [37], consisting of eleven detector modules, each containing four 36-fold segmented high-purity germanium crystals. GRETINA was arranged to cover the forward hemisphere, with four detector modules located at 58° and seven at 90° with respect to the beam axis. The spatial coordinates of the γ-ray interaction points within the GRETINA crystals were deduced from pulse-shape analysis of the digitized signal traces read out from each segment. The first interaction point, assumed to correspond to the coordinate with the largest energy deposition, was used to calculate the γ-ray emission angle with respect with the fragment's trajectory, which enters into the event-by-event Doppler reconstruction of the γ rays emitted in flight by the P isotopes. The parameters used for the Doppler reconstruction were determined using known transitions from other nuclei also transmitted to the focal plane of the S800 spectrograph. We used the 249.2(2)-keV transition in ^{36}P [38], the 1292.02(20)-keV transition in ^{38}S [39], and the 1351.10(14)-keV transition in ^{40}S [40] to extract the relevant parameters, such as the target offset, for this experiment. Much of the $\gamma\gamma$ coincidence analyses performed in this work employed addback, a procedure for recovering the full γ-ray energy of events scattered from one crystal into a direct neighbor as described in Ref. [41]. To determine $\gamma\gamma$ coincidence relationships for the placement of transitions within cascades in the level schemes, software cuts on γ-ray transitions in $\gamma\gamma$ coincidence matrices were employed with appropriate background subtraction.

Spectra were fitted using the results from a GEANT4 simulation [42, 43], with parameters adjusted to reproduce GRETINA's response to standard calibration sources at rest. The fits were used to obtain the relative γ-ray intensities, or branching ratios, from the peak areas. In some cases, the comparison of Doppler-broadened lineshapes of γ-ray transitions allowed us to deduce effective mean lifetimes in the range of hundreds to thousands of picoseconds which leave marked imprints on the Doppler-broadened lineshape. The fitted spectra in the following are shown without addback as addback has not been fully benchmarked in GEANT simulation on the level of spectrum modeling aimed for here.

III. RESULTS AND DISCUSSION

In this section, the results are presented for the spectroscopy of $^{37-42}$P. The proposed level schemes and transition strengths, if extracted, are compared to large-scale shell-model calculations using the SDPF-MU effective interaction [17]. The calculations employ the full *sd* and *fp* model space for protons and neutrons, respectively, and effective proton and neutron charges of $e_\pi = 1.35e$ and $e_\nu = 0.35e$ and standard spin and orbital proton and neutron g factors. The calculations were carried out with the code NuShellX [44]. The errors presented with the measured γ-ray energies and excited state lifetimes in this section consist of statistical uncertainties from the fits and systematic uncertainties associated with the parameters used in the Doppler correction, added in quadrature.

A. ^{37}P

The neutron-rich ^{37}P isotope has six more neutrons than the only stable isotope of the $Z = 15$ chain. Figure 2 shows the Doppler-reconstructed γ-ray spectrum over three energy ranges as measured with GRETINA for the ^{37}P reaction residues. The solid red lines correspond to the best fit of a linear combination of GEANT4 spectra simulated for the individual γ-ray transitions and a global double-exponential background. Lifetimes are deduced from fits by fixing the neighboring peaks and the background and fitting only the peak of interest with different simulated lifetimes. Delayed components for transitions from levels fed by longer-lived states are included in the fit, with the intensities of these components determined from the measured intensity of the feeder transition and the literature branching ratios. The dashed blue

lines show a fit using the same technique, but with no excited-state lifetimes included in the simulations. Figure 3 shows the fit residuals. The large residuals associated with the 439(1), 861(1)/869(1), 1182(2), and 1301(2)-keV peaks in the fit without lifetimes demonstrate the need for their inclusion to achieve a reasonable description of the spectrum.

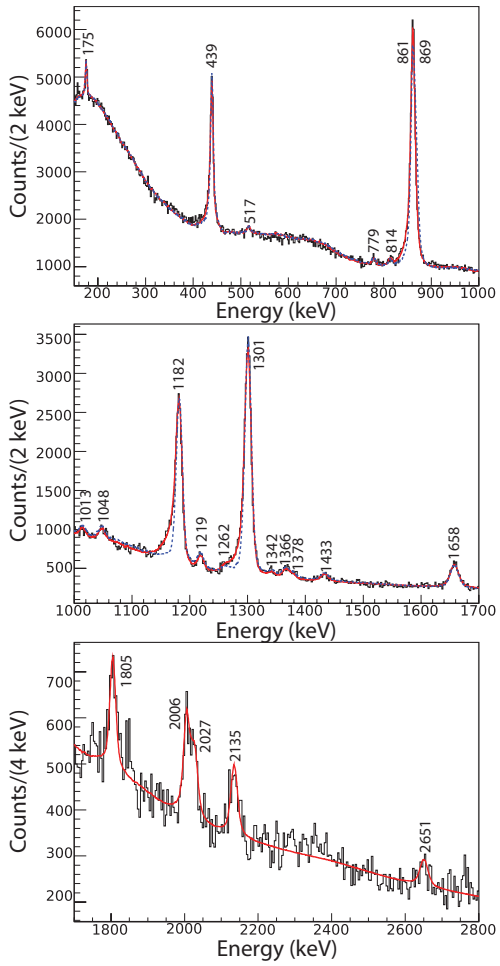

FIG. 2: Doppler-corrected (v/c = 0.340) γ-ray spectrum for ^{37}P as detected with GRETINA. The red lines correspond to GEANT4 simulations on top of an exponential background.The dashed blue lines in the top two panels shows the best fit if no excited-state lifetimes are included for the levels at 2483(2) and 3352(3) keV. The prominent lifetime effect visible for the 1182(2) and 1301(2)-keV transitions are a consequence of the feeding of their respective levels from the long-lived 3352(3)-keV state.

Intense transitions at 439(1), 861(1), 869(1), 1182(2), 1301(2), and 1658(3) keV, as well as a weaker γ ray at 1048(4) keV, were observed that can be identified with previously reported transitions. Also a strong peak at 175(1) keV is visible that appears to have been mislabeled as a contaminant from ^{36}P in the previous work by A. Hodsdon *et al.* [28]. The coincidence spectra support the previously reported level schemes for the first five

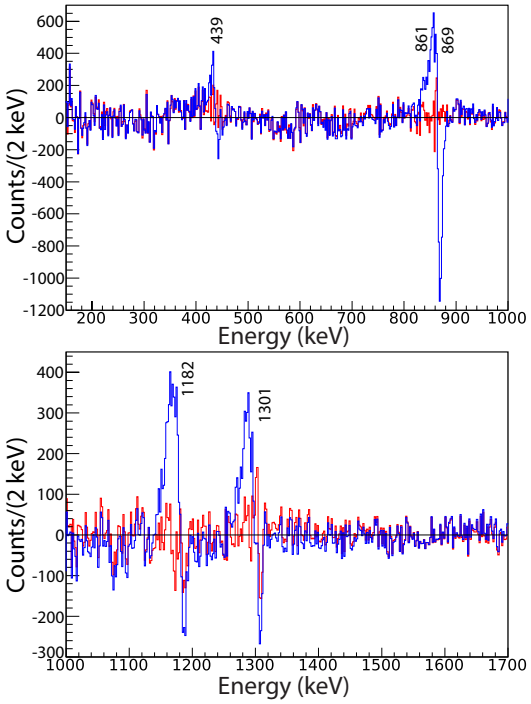

FIG. 3: ^{37}P residual spectra for the fits with lifetimes (red) and without lifetimes (blue) as shown in Figure 2. The large residuals in the latter fit correspond to the 869(1)-keV transition from the long-lived 3352(3)-keV state and all of the transitions from states fed by this state.

transitions mentioned above and offer strong evidence for new placements of the 1048(4) and 1658(3)-keV γ rays. Also, 15 additional transitions are reported here for the first time, eight of which could be placed in the level scheme. All 23 observed transitions are characterized in Table I.

Coincidence spectra for the observed γ-ray lines were used to inform the placements of transitions within the level scheme (Fig. 4). Figure 5 shows a selection of five coincidence spectra at the center of this analysis. Due to the close proximity of the 861(1) and 869(1)-keV transitions, the coincidences corresponding to these two transitions cannot be resolved separately. The energies of these two transitions are confirmed through a combination of their high sensitivity in the fit and energy differences with other well-known energies in the level scheme. They are also consistent with all previous measurements, including the low-uncertainty measurement by A. Hodsdon *et al.* [28].

The previous work by Hodsdon *et al.* tentatively placed the 1048(4) and 1658(3)-keV transitions in a cascade on top of the 869(1)-keV transition in the level scheme [28]. In the present work, the 1658(3)-keV transition indeed shows a strong coincidence with the 861(1)-keV line, but not with the other strong transitions that would be expected from this previous placement higher up in the level scheme. Accordingly, this transition is

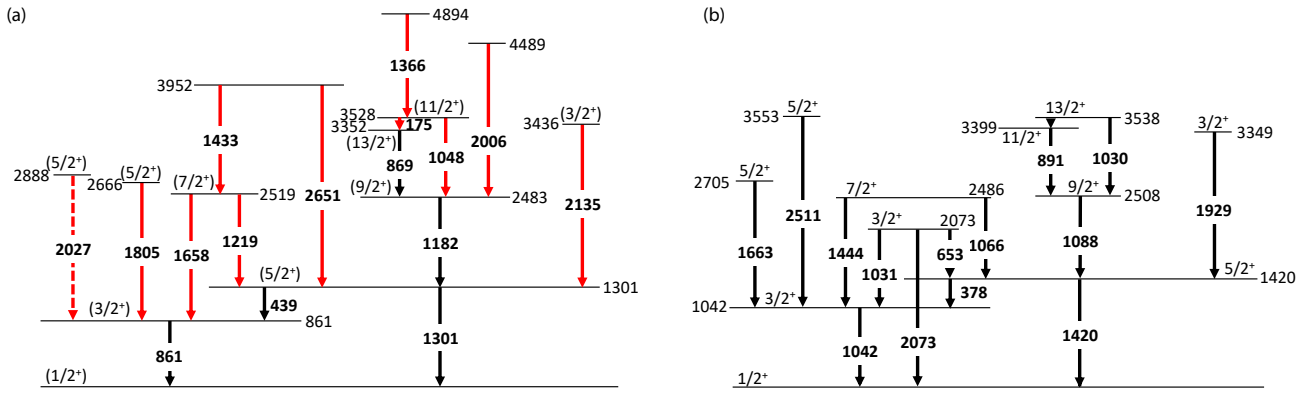

FIG. 4: (a) Proposed ^{37}P level scheme containing all placed transitions in the present measurement. Red arrows mark newly-placed transitions, and dashed arrows indicate tentative placements. (b) Predicted ^{37}P level scheme based on SDPF-MU shell-model calculations. All predicted levels up to 3553 keV are shown.

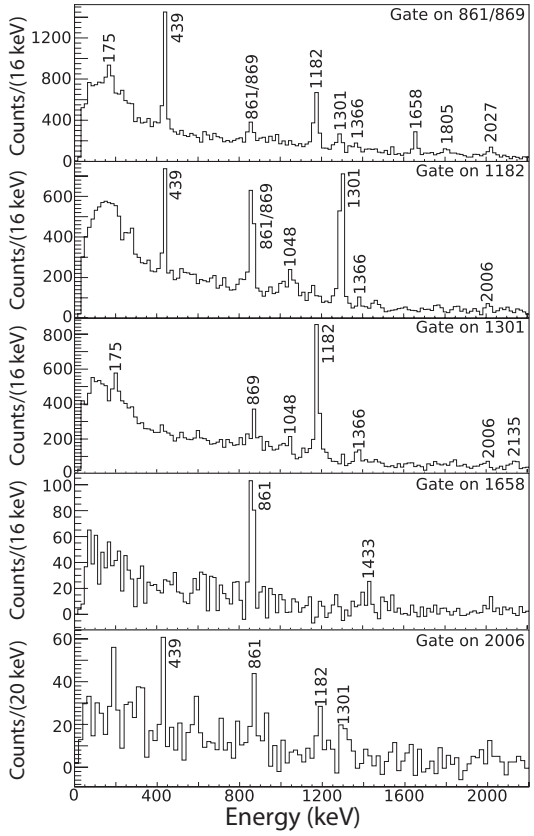

FIG. 5: Selected background-subtracted $\gamma\gamma$ coincidence spectra for ^{37}P.

placed directly atop the 861(1)-keV state. Coincidence relationships with the much weaker 1048(4)-keV line are less compelling, but that transition's strongest coincidence is with the 1182(2)-keV line and its energy fits into the level scheme as a decay from the 3528(3)-keV state, known from the well-defined placement in this work of the 175(1)-keV transition to the 3352(3)-keV state. The lack of coincidences with the 861(1)-keV transition is explained by the low intensity of the 1048(4)-keV transition in combination with the relatively small branching ratio of that decay path. The level energies associated with the new placements of these transitions are consistent with the excited states at 2570(30) and 3560(30) keV previously reported by Fifield *et al.* [27] from particle spectroscopy. The placement of the 2027(4)-keV transition is tentative due to limited statistics and difficulty separating its coincidences from the nearby 2006(3)-keV line. Seven of the observed transitions cannot be placed in the level scheme due to a combination of low statistics and close proximity to more intense peaks, preventing an unambiguous coincidence analysis.

Table I lists the observed ^{37}P energy levels together with their decays and other measured information. Spin-parity assignments are suggested from comparison with shell-model calculations using the SDPF-MU effective interaction. Figure 4 confronts the proposed ^{37}P level scheme with the predicted one. The theoretical level scheme shows all of the computed levels up to 3553 keV. The high level density above this energy makes it difficult to associate predicted states with measured ones. Newly placed transitions are marked in red in the level scheme proposed from the present data. The seven unplaced γ rays observed are not shown but are included in the table. The experimentally determined level scheme appears essentially complete up to the 3528(3)-keV level, aside from the $3/2^+_2$ state predicted at 2073 keV. Our new placements of the previously observed 1658(3) and 1048(4)-keV transitions may correspond to the calculated yrast $7/2^+$ and either the $11/2^+$ or the $13/2^+$ states. The shell-model calculation predicts only a small energy difference between the $11/2^+_1$ and $13/2^+_1$ levels and a similar decay pattern. The 3352(3) and 3528(3)-keV states are tentatively assigned as $(13/2^+)$ and $(11/2^+)$, respectively, based on predicted transition strengths, described

below.

Furthermore, constraints could be placed on the effective lifetime of the 3352(3)-keV state in ^{37}P from the observed Doppler line shape in this high-statistics case. The Doppler-corrected γ-ray line shape of the 869-keV peak, as well as those of the transitions from states it feeds, display left tails. To account for these peak shapes, lifetimes were included in the GEANT4 simulations of the GRETINA response. Due to the close proximity of the 861(1) and 869(1)-keV transitions, and with no way to independently constrain the intensity of the lower-energy peak, it was not possible to employ the preferred technique of fixing the background and neighboring peaks to only allow the lifetime and peak intensity to vary. Because of these complications, firm lifetimes for the states involved cannot reasonably be quoted and τ_{fit} is then rather treated as a lifetime-like variable to improve the fit that indicates the order of magnitude for τ. The best fit, shown in Fig. 2, was achieved using $\tau_{fit} = 75$ ps for the 3352(3)-keV state and $\tau_{fit} = 3$ ps for the 2483(2)-keV state. The fit also includes the associated delayed components for the prompt transitions from levels fed by these longer-lived states. Fitting without these lifetimes results in uncertainties on the order of 25% in the peak intensities. The inclusion of a small lifetime for the $9/2^+$ state is consistent with the SDPF-MU shell-model predictions. The $11/2^+$ and $13/2^+$ states have predicted lifetimes of only 3 and 13 ps, respectively, which are smaller than the fit variable $\tau_{fit} = 75$ ps that may compensate for other unconstrained effects in the regime of intense neighboring peaks.

Since the 3352(3)-keV state cannot confidently be assigned as either the $11/2^+_1$ or the $13/2^+_1$ state from the level scheme alone, the order of magnitude of the transition strengths from the lifetime estimate for both possibilities is considered. If the level is the $13/2^+_1$ state, the transition to the $9/2^+_1$ level must be a pure $E2$ transition. Our estimated lifetime would yield a $B(E2; 13/2^+ \rightarrow 9/2^+)$ values of order 22 e^2fm^4. The SDPF-MU shell-model calculations predict the corresponding $B(E2)$ strength to be 21.7 e^2fm^4. Alternatively, if the level was the $11/2^+_1$ state, it may decay by either an $M1$ or $E2$ transition to the $9/2^+$. Using the multipole mixing ratio of $\delta = -0.04$ predicted by the shell-model calculations gives a $B(M1; 11/2^+ \rightarrow 9/2^+)$ strength of the order of 0.0012(1) μ_N^2, a factor of 20 smaller than the predicted 0.026 μ_N^2. This suggests that the 3352(3)-keV state may be the $13/2^+_1$ rather than the $11/2^+_1$ level.

B. ^{38}P

The odd-odd nucleus ^{38}P isotope is much less studied than its even-N neighbors. Previous spectroscopy of this nucleus is limited to a single transition observed in a projectile fragmentation experiment [30] and three transitions observed following the selective population of 1^+ excited states in the β decay of ^{38}Si [29]. Figure 6 shows the fitted, Doppler-reconstructed γ-ray spectrum measured in coincidence with the ^{38}P reaction residues. An intense γ-ray transition at 380(1) keV is visible and can be identified with the previously reported γ ray from Chapman *et al.* [30]. In addition, 20 transitions are reported for the first time. All but two of the observed transitions were placed in the level scheme. All 21 observed transitions are documented in Table II with the corresponding excited states characterized.

Although it is not immediately apparent from the spectrum alone, a doublet of transitions at 380(1) and 384(1) keV is strongly suggested, originating from levels with rather different excited-state lifetimes. The coincidence spectra for higher-lying states, shown in Fig. 7 and 8, are used to construct the level scheme (Fig. 9) around these two proposed states. Summing up the energies associated with various cascades suggests two distinct states rather than a single one. The 520(1)-keV level can decay with either a transition directly to the ground state or with a 136(1)-keV decay, indicating a state at 384 keV. The decays from the 1152(2)-keV level similarly place the state at 385 keV. The 1365(2)-keV state, however, can decay by a 984(2)-keV transition, suggesting instead a level at 381 keV. The low uncertainties on these transition energies makes it unlikely that these are

TABLE I: Energy levels and associated γ-ray transitions observed in ^{37}P. Tentative spin-parity assignments, branching ratios, and relative intensities of all transitions are given.

E_{level} [keV]	J^π	E_γ [keV]	Branching	Intensity
861(1)	$(3/2^+)$	861(1)	100	84.5(1.1)
1301(1)	$(5/2^+)$	439(1)	32(1)	32.1(0.8)
		1301(2)	100(1)	100.0(0.9)
2483(2)	$(9/2^+)$	1182(2)	100	73.6(1.6)
2519(2)	$(7/2^+)$	1219(2)	41(3)	5.7(0.4)
		1658(3)	100(3)	14.0(0.4)
2666(4)	$(5/2^+)$	1805(4)	100	6.5(0.4)
2888(4)	$(5/2^+)$	2027(4)	100	4.6(0.4)
3352(3)	$(13/2^+)$	869(1)	100	30.6(0.9)
3436(4)	$(3/2^+)$	2135(4)	100	5.3(0.4)
3528(3)	$(11/2^+)$	175(1)	100(10)	4.2(0.4)
		1048(4)	88(10)	3.7(0.4)
3952(4)	-	1433(3)	100(9)	3.5(0.3)
		2651(5)	80(11)	2.8(0.4)
4489(4)	-	2006(3)	100	6.6(0.4)
4894(4)	-	1366(3)	100	4.4(0.4)
-	-	517(2)	-	1.8(0.3)
-	-	779(2)	-	2.6(0.3)
-	-	814(3)	-	2.5(0.3)
-	-	1013(1)	-	2.9(0.4)
-	-	1262(5)	-	1.9(0.3)
-	-	1342(2)	-	2.5(0.3)
-	-	1378(5)	-	2.2(0.4)

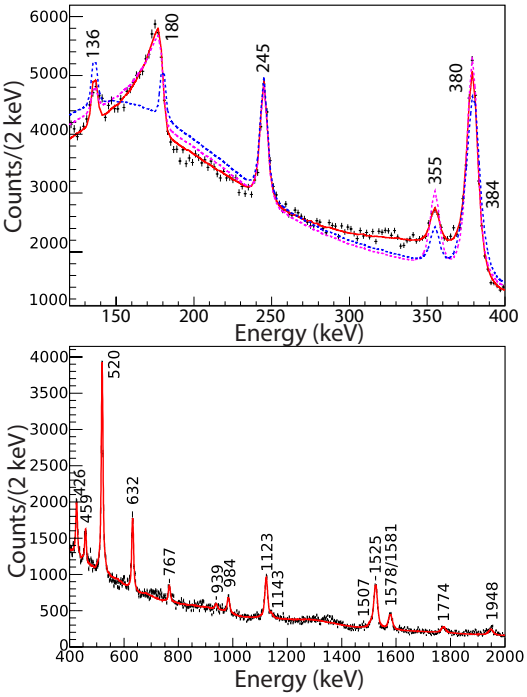

FIG. 6: Doppler-corrected ($v/c = 0.333$) γ-ray spectrum detected with GRETINA in coincidence with ^{38}P as identified with the S800 spectrograph. The red line represents the GEANT4 response functions on top of an exponential background fit to the data. In the top panel, the dashed blue line shows the best fit if no excited-state lifetimes are included and the dashed magenta lines shows the best fit including lifetimes, but excluding the transition at 384 keV.

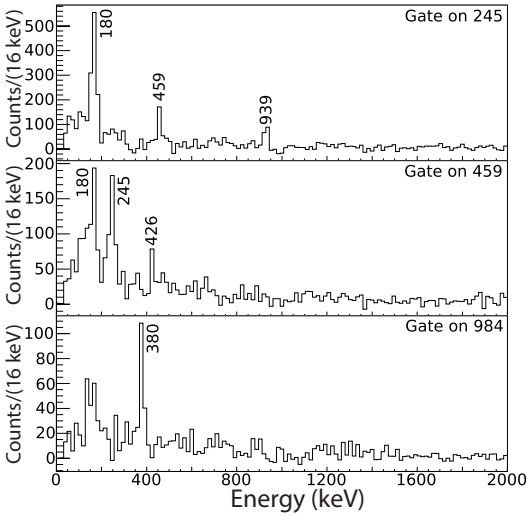

FIG. 7: Background-subtracted $\gamma\gamma$ coincidence spectra for ^{38}P, gated on transitions in the structure shown on the left in Fig. 9.

a single peak, particularly because fitting a single peak places the best fit energy at 380(1) keV. Fitting two peaks places the best-fit energies at 380(1) and 384(1) keV, consistent within uncertainty with the cascade energies. Additionally, the coincidences for transitions which feed the 380(1)-keV state in our proposed level scheme, shown in the bottom panel of Fig. 7 and 8, display a narrow peak in this region, while those for the transitions which feed the proposed 384(1)-keV state, in the third and fourth panels of Fig. 8, show a much broader one. This is consistent with the suggested lifetime effect associated with the latter state, which results in a broadening of its γ-ray lineshape compared to the proposed prompt decay of the 380(1)-keV state. Note that while the doublet at 1578(4)/1581(4) keV is in coincidence with both transitions, most of its intensity decays to the 380(1)-keV state, consistent with the narrow peak in its coincidence spectrum. We also find that a single transition cannot accurately fit the spectrum in this region, regardless of the energy or lifetime used. The magenta line in Fig. 6 shows the best fit achievable without the inclusion of a long-lived 384(1)-keV transition. The underestimation of the "background" in this fit is the result of the required long lifetime, $\tau = 2670(250)$ ps, which causes a substantial and extended low-energy tail. Coincidences taken with the region from 280 to 330 keV, which corresponds to the long tail of the proposed isomeric transition at 384(1) keV, are roughly consistent with the existence of the doublet and the placement of the two transitions in the level scheme, although the low signal-to-background ratio in this region makes a coincidence analysis difficult. The inclusion of two states is also supported by the SDPF-MU shell-model calculation for ^{38}P, which predict both the 3^-_1 and 4^-_1 states to be at low energies, with the 4^-_1 state calculated to have a lifetime on the order of hundreds of picoseconds due to the $E2$ character of its decay to the 2^- ground state. The expected decays and feeding patterns of these states are also consistent with our proposal. Furthermore, if the 384(1)-keV state is not included in our level scheme, no other observed state is consistent with the predicted 4^-_1 level.

The close proximity of the 380(1) and 384(1)-keV transitions, combined with the latter's Doppler broadening, makes resolving coincidence relationships in this region very difficult. Since both transitions appear to be decays leading to the ground state directly, their feeders are proposed by examination of energy differences between the higher-lying transitions in addition to the coincidence spectra.

Figure 9 compares the ^{38}P level scheme with the SDPF-MU shell-model calculations. The experimental scheme shows newly placed transitions in red. The observed level scheme has two unlinked structures, consistent with the shell-model predictions. Curiously, within the shell model, there is no marked difference in the configurations of the states that belong to the disconnected structures and the lack of linking transitions may be solely rooted in energy and spin differences, suppressing decay branches between them. The state proposed

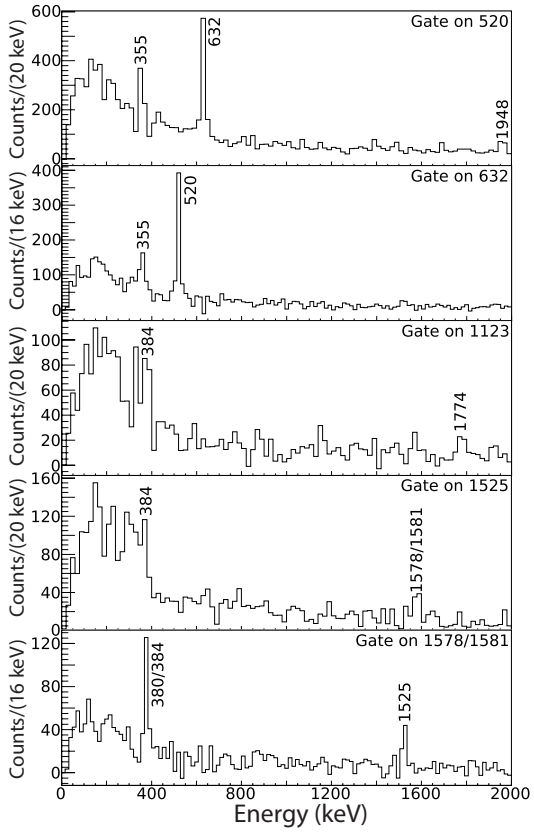

FIG. 8: Background-subtracted $\gamma\gamma$ coincidence spectra for ^{38}P, gated on transitions in the structure on the right in Figure 9.

at 885 keV has no correspondence in the shell model. Tentative spin assignments are associated with experimental levels through comparisons of energies, decays, feeders, branching ratios, and lifetimes with the results from shell-model calculations. The high predicted level density above 1500 keV makes suggestions of spin values for higher-lying states difficult. The observed level energies and ordering of states for ^{38}P differ from the predicted values much more than for even-N ^{37}P, which is not unexpected given that the description of the proton-neutron couplings in odd-odd nuclei is more demanding for the Hamiltonian.

We report the peak structure at approximately 1580 keV as a doublet. The coincidence spectra for this doublet, in Fig. 8, show only the 380(1)/384(1) and 1525(3)-keV transitions. This, combined with the placement of the other transitions in the level scheme, suggests a cascade with the 1525(3) and 384(1)-keV transitions. However, the number of coincidence counts for the 1525(3)-keV transition is roughly a third of what would be expected in this scenario. Additionally, the narrow peak at 380 keV suggests that the doublet is coincident primarily with the fast 380(1)-keV transition, and not the long-lived 384(1)-keV transition which would show substantial broadening of the γ-ray lineshape.

Assuming two peaks in the fit leads to energies at 1578(4) and 1581(4) keV. Despite their relatively high intensities, the placements of those two transitions in the level scheme remain tentative due to the inability to resolve their coincidences separately, and the difficulty of resolving the 380(1) and 384(1)-keV transitions in the coincidence spectra. A previously observed transition at 1120(2) keV was tentatively placed as a ground-state transition from a 1^+ state by Tripathi *et al.* [29], with the spin-parity assignment informed by allowed β-decay selection rules. The 1123(2)-keV transition observed here is placed as a decay to the 384(1)-keV state based on the observed coincidence. Low statistics in the previous measurement may explain the non-observation of the 384(1)-keV transition. However, the 1507(2)-keV level, from which this transition originates, is most similar to the predicted 5^- level in the SDPF-MU shell-model calculations (which for ^{38}P includes only negative parity states within the given model space). Since the β decay from the 0^+ ground state of ^{38}Si to a 5^- state is highly suppressed, it is likely that the present work and [29] observe different transitions that happen to have similar energies. The 1507(3)-keV transition is not placed in the level scheme despite an observed level at that energy because this would require the transition to be of $M3/E4$ multipolarity.

Clear lifetime effects are visible in the γ-ray spectra for the 180-keV transition and, when considering the alternative fits in Fig. 6, for the doublet around 380 keV as well. Excited-state lifetimes are extracted for the corresponding states at 180(1), 380(1), and 384(1) keV, using the γ-ray lineshape analysis technique described previously. The 180(1)-keV lifetime was determined by fixing the background and nearby transitions and varying only the lifetime and peak area. This fit is shown in Fig. 10.

Extracting the lifetimes for the 380(1) and 384(1)-keV states is more complicated since the two peaks overlap. The 384(1)-keV transition is broad enough to impact the spectrum down to about 200 keV. In order to assess the lifetime, first all other fit components in the region were fixed. The two prompt peaks in the region of interest, corresponding to the 245(1) and 355(1)-keV transitions, were fitted with a free double-exponential background parameter to account for both the actual background and the counts from the tail of the long-lived 384(1)-keV transition. A scalable background template was constructed by subtracting all fitted peaks from the spectrum of ^{39}P shown in the next section. This template was then scaled by fitting it both to the 120-200 and 400-600-keV regions of the ^{38}P spectrum. This procedure of fixing the background only leaves the energies, lifetimes, and intensities of the two peaks of interest as free parameters and increased the sensitivity of the fit to the peak shape of the 384(1)-keV transition. The 380(1)-keV transition energy has been reported previously with an uncertainty of 1 keV by Chapman *et al.* [30] and this precise energy was used here. The 384(1)-keV transition has not previously been observed, but its energy is tightly constrained by

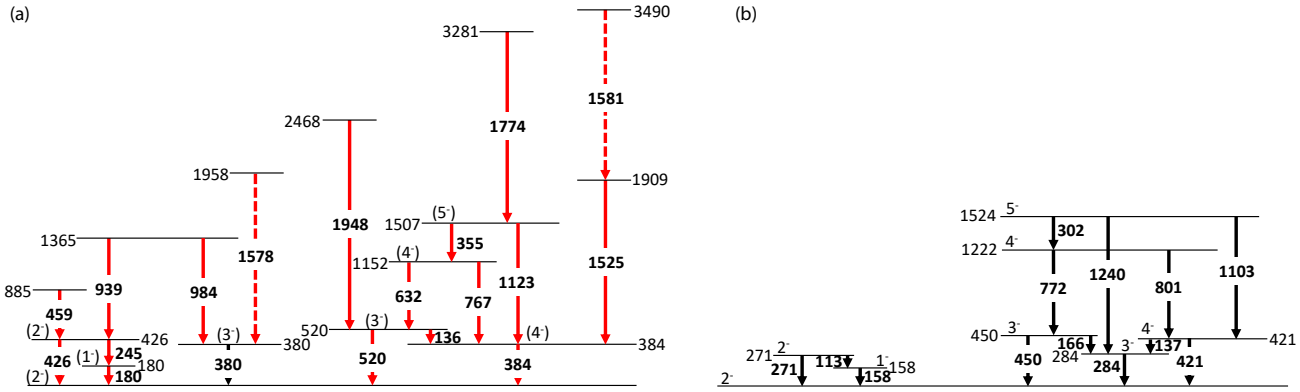

FIG. 9: (a) Proposed ^{38}P level scheme containing all placed transitions in the present measurements. Red arrows mark newly-placed transitions, and dashed arrows indicate tentative placements. (b) Predicted ^{38}P level scheme based on SDPF-MU shell-model calculations. All predicted negative-parity states up to 1524 keV are shown.

its placement in the level scheme. The first instance of fitting varied the lifetimes, the intensities, and the 384(1)-keV transition energy while fixing all other parameters. For any reasonable combination of lifetimes, it was found that the energy χ^2 fit of the longer-lived state has a sharp minimum at 384 keV. This then allowed all transition energies to be fixed and left the two lifetimes and intensities as the only free parameters.

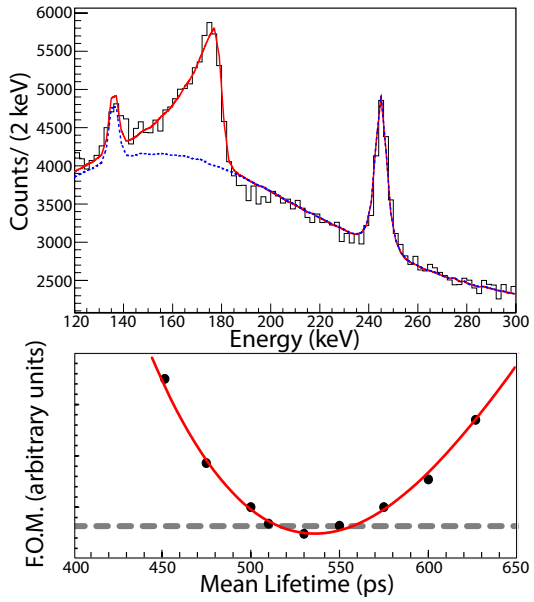

FIG. 10: The upper panel shows the fit for the lifetime analysis of the 180(1) keV transition in ^{38}P. The background and all other transitions were fixed (represented by the blue line) and only the lifetime and peak area were varied. The total resulting best fit is shown in red. The lower panel shows the figure of merit of the fit as a function of the simulated lifetime. The dashed line corresponds to the 95% confidence interval. The best fit lifetime is 536(32) ps.

The dramatic broadening of the γ-ray line shape of the 384(1)-keV transition leads to a large energy range where the peaks do not overlap despite the similar energies. As a result, the correlation between the two lifetimes is weak. For any reasonable lifetime choice for the 384(1)-keV transition, one finds that the best fit for the lifetime of the 380(1)-keV line is 22(3) ps. This conveniently allows this parameter to be fixed and reduces the fit to only the two peak intensities and the lifetime of the 384(1)-keV transition. Once the best-fit lifetimes for both transitions were obtained, the longer lifetime was fixed and the energy and lifetime of the 380(1)-keV transition was varied to confirm the fit energy. Shifting this transition energy by only 1 keV in either direction results in a substantially worse fit, supporting our initial assumption.

From comparison to shell model, the three longer-lived states at 180(1), 380(1), and 384(1) keV are associated with the predicted 1^-_1, 3^-_1, and 4^-_1 levels, respectively. The SDPF-MU shell-model calculations predict lifetimes of 464 ps for the 1^-_1 state and 39 ps for the 3^-_1 state, which are roughly consistent with our measurements of 536(32) ps and 22(3) ps, respectively. The predicted lifetime for the 4^-_1 state is 255 ps, which is an order of magnitude smaller than our measured value of 2670(250) ps. This discrepancy can possibly be explained by differences between the predicted and observed energies and branching ratios. The shell model predicts that this state should decay to the 3^-_1 state 80% of the time, but our observed states are separated by only 4 keV as opposed to the predicted 137 keV. This makes a transition between those two states much less likely, leaving only the decay to the ground state as a low-multipolarity transition. The shell model also predicts a lifetime of 140 ps for the 2^-_2 state, but the two transitions originating from this state appear to be prompt. This discrepancy is at least partially explained by the much higher energy of the observed state (426 keV as opposed to 271 keV in the calculation).

Transition strengths are computed from experiment and compared to shell-model calculations. The decay from the 384(1)-keV (4^-) state to the (2^-) ground state is a pure $E2$ transition, giving a $B(E2;(4^-)\rightarrow(2^-))$ value of 37(3) $e^2\mathrm{fm}^4$. The shell-model calculations predict a $B(E2;4^-\rightarrow 2^-)=32\ e^2\mathrm{fm}^4$. The other two longer-lived states may decay by either $M1$ or $E2$ multipolarity, but the predicted mixing ratios are -0.06 and <0.01 for the 180(1) and 380(1)-keV transitions, respectively, indicating nearly pure $M1$ character. Using these mixing ratios yields $B(M1;(1^-)\rightarrow(2^-))=0.018(1)\ \mu_N^2$ as compared to the predicted transition strength of 0.031 μ_N for the decay of the 1^- state. For the 380(1)-keV (3^-) level we compute a $B(M1;(3^-)\rightarrow(2^-))$ value of 0.047(6) μ_N^2 as compared to the predicted one of 0.064 μ_N^2.

C. ^{39}P

Figure 11 shows the fitted, Doppler-reconstructed γ-ray spectrum taken in coincidence with the ^{39}P reaction residues. Intense γ-ray transitions are observed at 355(1), 618(2), 973(1), and 1210(2) keV that can be identified with previously reported γ rays from an intermediate-energy Coulomb excitation experiment [26], a ^{40}Si β-decay experiment [29], and a projectile fragmentation experiment [31]. Sixteen additional transitions are reported here for the first time.

TABLE II: Energy levels and associated γ-ray transitions observed in ^{38}P. Tentative spin assignments, branching ratios and relative intensities of all transitions are given.

E_{level} [keV]	J^π	τ (ps)	E_γ [keV]	Branching	Intensity
180(1)	(1^-)	536(32)	180(1)	100	57.5(1.0)
380(1)	(3^-)	22(3)	380(1)	100	40.8(0.5)
384(1)	(4^-)	2670(250)	384(1)	100	100.0(1.6)
426(1)	(2^-)	-	245(1)	100(3)	16.0(0.4)
			426(1)	61(3)	9.7(0.4)
520(1)	(3^-)	-	136(1)	23(2)	10.2(0.7)
			520(1)	100(1)	44.0(0.5)
885(1)	-	-	459(1)	100	6.7(0.3)
1152(1)	(4^-)	-	632(1)	100(3)	19.5(0.5)
			767(2)	28(2)	5.4(0.4)
1365(2)	-	-	939(2)	34(6)	2.3(0.4)
			984(2)	100(7)	6.8(0.5)
1507(2)	(5^-)	-	355(1)	35(1)	7.3(0.3)
			1123(2)	100(2)	21.1(0.5)
1909(3)	-	-	1525(3)	100	34.2(0.7)
1958(4)	-	-	1578(4)	100	8.0(1.6)
2468(4)	-	-	1948(4)	100	6.3(0.5)
3281(4)	-	-	1774(4)	100	5.8(0.5)
3490(5)	-	-	1581(4)	100	4.6(1.6)
-	-	-	1143(5)	-	1.6(0.4)
-	-	-	1507(3)	-	2.6(0.5)

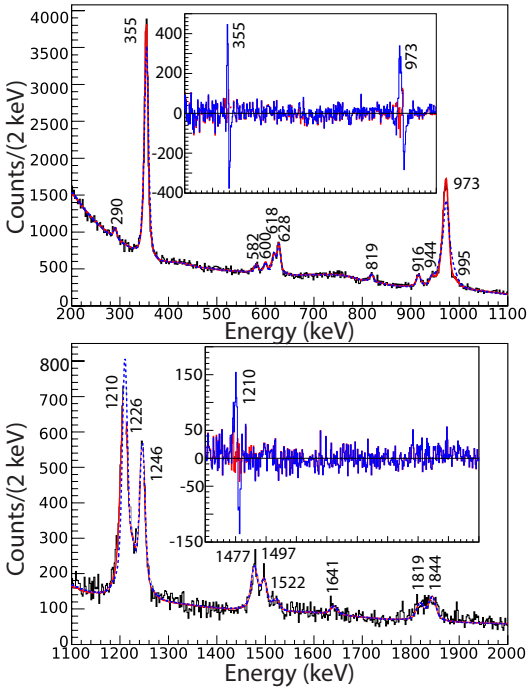

FIG. 11: Doppler-corrected (v/c = 0.333) γ-ray spectrum detected with GRETINA in coincidence with ^{39}P as identified with the S800 spectrograph. The red line represents the GEANT4 fit to the data. This fit includes delayed components for the transitions whose levels are fed by long-lived states. The dashed blue line shows the best fit if no excited-state lifetimes are included for the 355(1), 973(1), or 2183(2) keV levels. The insets show the residual spectra for the fits including (red) and excluding (blue) excited-state lifetime effects. The large residuals in the latter fit correspond to the 355(1), 973(1), and 1210(2) keV transitions, which we thus associate with lifetime effects

The coincidence spectra for this nucleus, shown in Fig. 12, are consistent with the previous placements of the known transitions and enable placement of ten of the newly observed transitions as well. Figure 13 compares the ^{39}P level scheme with the SDPF-MU shell-model calculations. The depicted theoretical scheme includes all calculated energy levels up to 2496 keV. The levels at 3073 and 3100 keV are also included because they are the only two calculated levels with similar properties to the observed state at 3098(2) keV. Based on the predicted branching ratios, the measured level is more likely the $11/2^+$ state. The placement of the 944(1)-keV transition is tentative due to low statistics. The level scheme proposed from experiment appears complete up to the 2199(3)-keV level; it exhausts all predicted states up to 2496 keV, and the predicted energies, particularly for the yrast states, are rather similar to the measured ones.

The 973(1)-keV state has been observed in three separate experiments prior to this work [26, 29, 31]. A relative branching ratio of 9(1) for the 618(2)-keV transition from this state is deduced, which is substantially

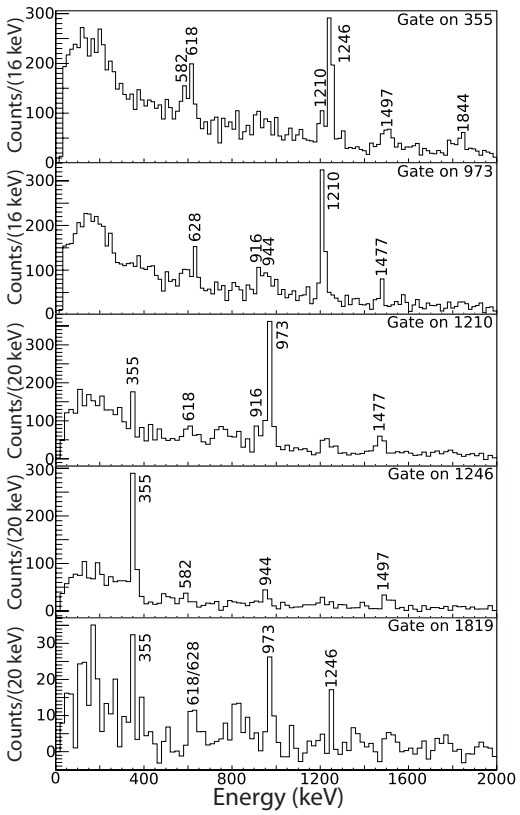

FIG. 12: Background-subtracted $\gamma\gamma$ coincidence spectra for ^{39}P.

smaller than the previous measurement by O. Sorlin *et al.* [31] of 67. However, our result is consistent with the non-observation of this transition in two previous experiments that report the ground-state transition from this state [26, 29]. Our measured branching ratio is also in agreement with the shell-model prediction of a branching ratio of 9 for the decay to the $3/2^+$ excited state relative to the decay $1/2^+$ ground state.

A γ-ray line shape analysis suggests short lifetimes for the 355(1), 973(1), and 2183(2)-keV states. This analysis is possible for these short lifetimes due to the combination of high statistics and low energy uncertainty achieved in this experiment. The overall fit is substantially improved by including lifetimes of τ_{fit} = 21, 6, and 16 ps, respectively, for these states. If the spectrum is fit without these lifetimes, the difference in γ-ray lineshapes between simulation and data results in an uncertainty on the order of 50% in the intensity of the 355(1) and 973(1) keV transitions, and on the order of 10% for the 1210(2) keV transition. The insets in Fig. 11 show the residual spectra from the fits with and without the lifetime effects. The large residuals associated with the 355(1), 973(1), and 1210(2)-keV transitions in the fit without lifetime effects demonstrates the need for the inclusion of lifetimes to achieve a reasonable fit. We do not report these lifetimes as actual measurements due to the systematic, uncontrolled uncertainties associated with using this technique for such short lifetimes and the proximity of other transitions to the peaks of interest. However, the inclusion of these lifetimes in the fits is consistent with the SDPF-MU shell-model calculations, which predict lifetimes of 9, 19, and 7 ps for these levels, respectively. No other longer-lived states are predicted.

TABLE III: Energy levels and associated γ-ray transitions observed in ^{39}P. Tentative spin assignments, branching ratios, and relative intensities of all transitions are also given.

E_{level} [keV]	J^π	E_γ [keV]	Branching	Intensity
355(1)	$(3/2^+)$	355(1)	100	73.7(1.7)
973(1)	$(5/2^+)$	618(2)	9(1)	9.2(0.6)
		973(1)	100(2)	100(2.0)
1601(1)	$(7/2^+)$	628(1)	42(2)	14.0(0.7)
		1246(2)	100(3)	33.1(1.1)
2183(2)	$(9/2^+)$	582(1)	7(1)	3.9(0.5)
		1210(2)	100(2)	52.5(0.9)
2199(3)	$(5/2^+)$	1226(3)	64(7)	5.8(0.6)
		1844(4)	100(7)	9.1(0.6)
2545(2)	-	944(1)	100	6.3(0.6)
3098(2)	$(11/2^+)$	916(1)	99(6)	8.1(0.5)
		1497(3)	100(7)	8.2(0.6)
3420(4)	-	1819(4)	100	6.2(0.6)
3660(3)	-	1477(3)	100	11.7(0.7)
-	-	290(1)	-	2.8(0.4)
-	-	600(2)	-	4.3(0.5)
-	-	819(1)	-	4.7(0.5)
-	-	995(3)	-	1.7(0.6)
-	-	1522(4)	-	3.1(0.6)
-	-	1641(3)	-	2.6(0.5)

D. ^{40}P

Previous spectroscopy of ^{40}P is limited to the selective population of 1^+ excited states in the β decay of ^{40}Si [29]. The statistics for ^{40}P are roughly two orders of magnitude lower than for the lighter phosphorus isotopes and the information extracted from the present data is thus more limited. Figure 14 shows the fitted, Doppler-reconstructed γ-ray spectrum taken in coincidence with the ^{40}P reaction residues. Eight γ-ray transitions are observed, none of which have been reported previously.

Five of the observed transitions could be placed in the level scheme. Figure 15 compares the ^{40}P level scheme with the SDPF-MU shell-model calculations. The transition labeled with energy 'x' in the experimental scheme represents an unobserved decay that appears to have to exist from the 289(1)-keV state. Figure 16 shows a clear coincidence between the 289(1) and 545(1)-keV lines and no other observed transitions. The 289(1)-keV transition

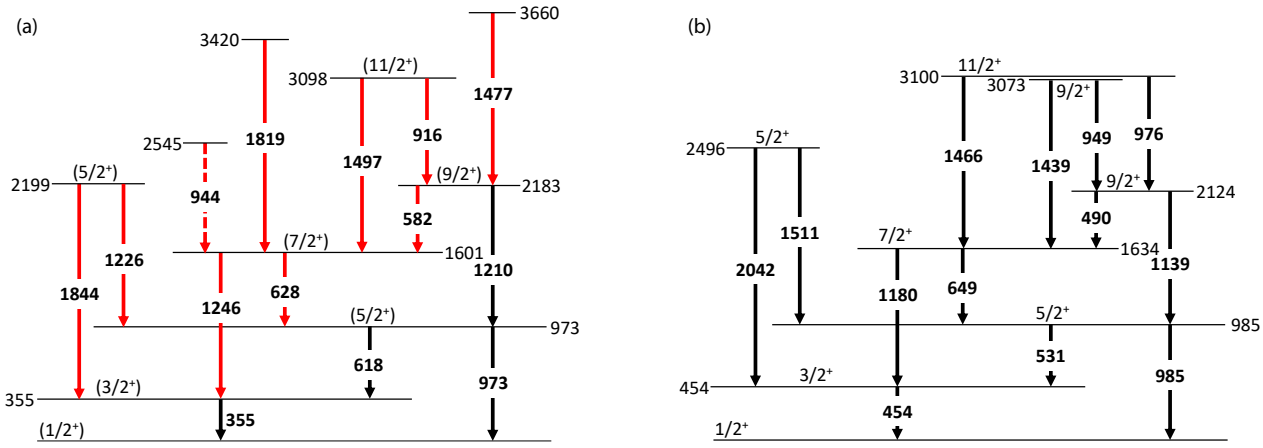

FIG. 13: (a) Proposed ^{39}P level scheme containing all placed transitions in the present measurements. Red arrows indicate newly-placed transitions, and dashed arrows indicate tentative placements. (b) Predicted ^{39}P level scheme based on SDPF-MU shell model calculations. All predicted levels up to 2496 keV are shown, as well as two levels at 3073 and 3100 keV that we associate with an observed level at 3098(2) keV.

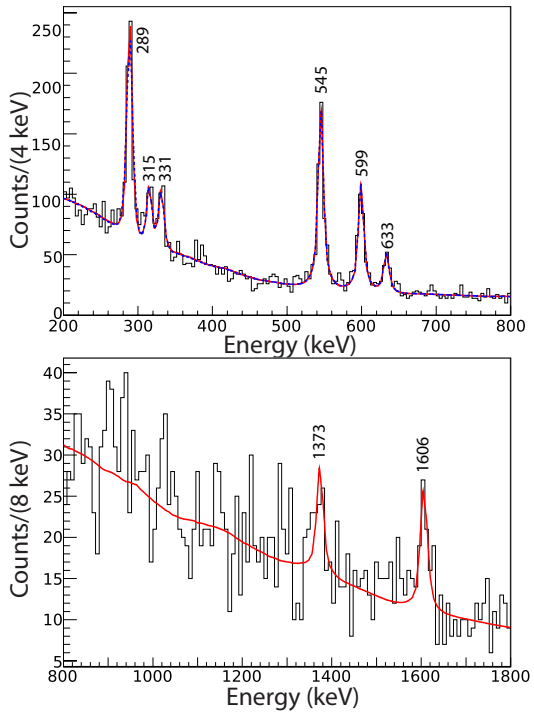

FIG. 14: Doppler-corrected (v/c = 0.331) γ-ray spectrum detected with GRETINA in coincidence with ^{40}P as identified with the S800 spectrograph. The red line represents a GEANT4 fit to data. The dashed blue line in the top panel shows the best fit if no lifetime is included for the 289(1) keV transition.

is best fit with a mean lifetime of 15 ps, and there is no evidence of a correspondingly delayed component for the 545(1)-keV transition, indicating that the higher-energy transition must be the feeder. However, the intensity of the 545(1)-keV transition is more than four standard deviations greater than that of the 289(1)-keV transition. It is thus likely that there is intensity missing in the decays depopulating the 289(1)-keV state. The low statistics, combined with both the Doppler broadening of the γ-ray line shape due to the parent state lifetime as well as the high background at low energies, could lead to the non-observation of another low-energy decay from this state. The shell-model calculation also predicts that the first excited state is longer-lived with an energy of 321 keV and a lifetime of 86 ps. This could be a possible end point of the transition suspected missing from the 289(1)-keV state.

Coincidence relationships for the 331(1), 599(2), and 633(1)-keV γ rays suggest a cascade. There are insufficient statistics to determine placement of the remaining three transitions. Unlike for the other P isotopes reported here, the predicted level scheme for ^{40}P is not easily comparable to the experimentally observed one. Therefore, no proposed spin assignments for our measured levels can be offered from comparison to shell model.

E. ^{41}P

As for ^{40}P, the statistics for ^{41}P are limited as compared to the lighter P isotopes with $A = 37 - 39$. Figure 17 shows the fitted, Doppler-reconstructed γ-ray spectrum from the ^{41}P reaction residues. Identified are γ-ray transitions at 172(1), 443(2), 731(2), 972(4), 1148(4), and 1420(4) keV that can be associated with previously reported transitions from two prior fragmentation experiments [6, 32], as well as a new transition at 1405(5) keV. The experiment by Riley *et al.* also reported a transition at 1729(5) keV [32], not seen in this measurement.

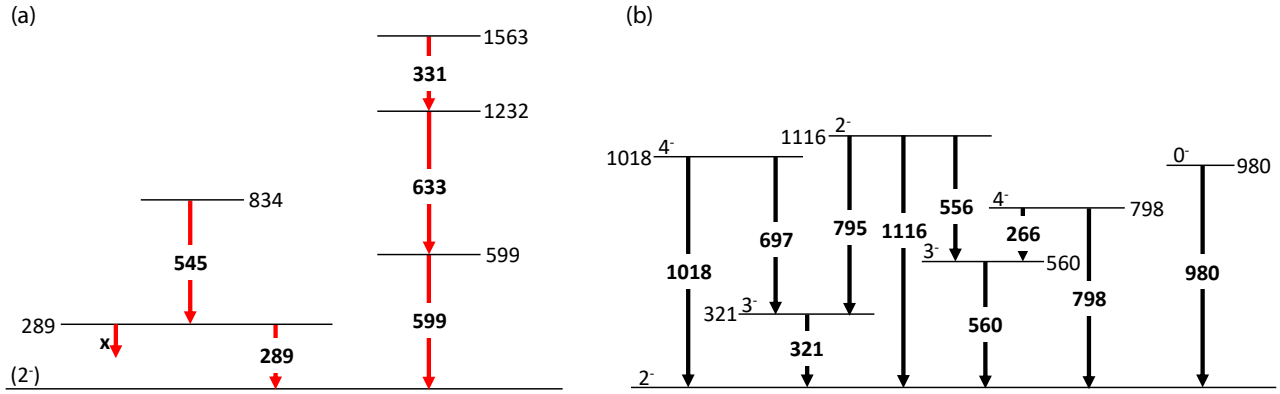

FIG. 15: (a) Proposed ^{40}P level scheme containing all placed transitions in the present measurements. Red arrows indicate newly-placed transitions. The transition marked with an 'x' represents the missing decay intensity from the 289(1)-keV state. (b) Predicted ^{40}P level scheme based on SDPF-MU shell-model calculations. All predicted levels up to 1116 keV are shown.

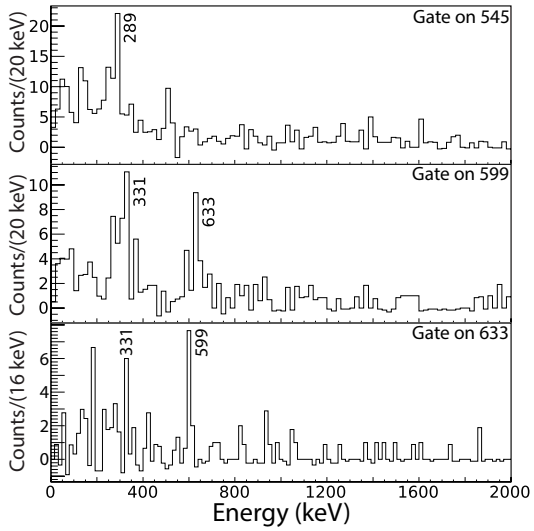

FIG. 16: Background-subtracted $\gamma\gamma$ coincidence spectra for ^{40}P.

Figure 18 compares the ^{41}P level scheme with the SDPF-MU shell-model calculations. The coincidence spectra for the 172(1)-keV transition in Fig. 19 shows the expected coincidence relationships given the previously reported level scheme for ^{41}P [6, 32]. Statistics for the other transitions were insufficient for a coincidence analysis. Bastin *et al.* placed a 420(22)-keV transition connecting states at 1574(19) and 1145(17) keV [6]. The 443(2)-keV transition reported here would fit well into the level scheme as a decay from the 1592(4) to the 1148(4)-keV state, and the existence of this branch would be consistent with the shell-model predictions for the $7/2^+_1$ level. However, the more recent measurement by Riley *et al.* did not observe any evidence for this transition and concluded that, if it originates from the 1592(4)-keV state, it must have a branching ratio of less

TABLE IV: Energy levels and associated γ-ray transitions observed in ^{40}P. The branching ratio for the 289(1) keV state is unknown due to missing decay intensity. Branching ratios and relative intensities of all transitions are given.

E_{level} [keV]	J^π	E_γ [keV]	Branching	Intensity
289(1)	-	289(1)	*	75.1(4.6)
599(2)	-	599(2)	100	64.5(5.2)
834(1)	-	545(1)	100	100.0(5.9)
1232(2)	-	633(1)	100	25.1(4.0)
1563(2)	-	331(1)	100	22.5(3.4)
-	-	315(2)	-	21.5(3.3)
-	-	1373(5)	-	13.5(4.3)
-	-	1606(5)	-	19.2(4.9)

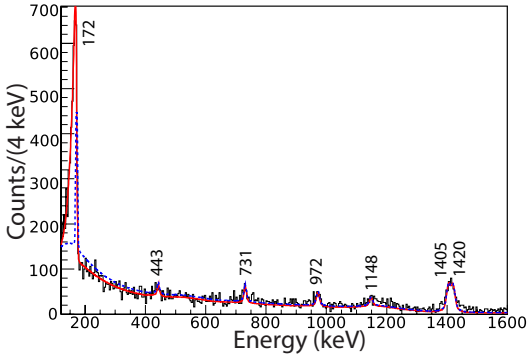

FIG. 17: Doppler-corrected (v/c = 0.328) γ-ray spectrum detected with GRETINA in coincidence with ^{41}P as identified with the S800 spectrograph. The red line represents the GEANT4 fit to data. The dashed blue line shows the best fit if no excited-state lifetime is included for the 172(1) keV transition.

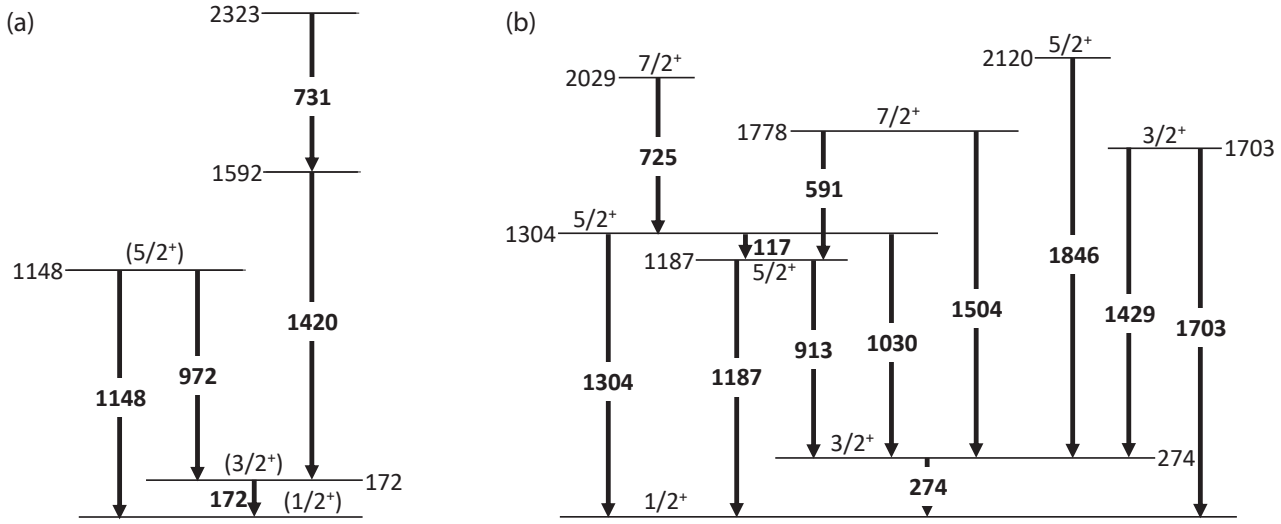

FIG. 18: (a) Proposed ^{41}P level scheme containing all placed transitions in the present measurements. (b) Predicted ^{41}P level scheme based on SDPF-MU shell model calculations. All predicted levels up to 2120 keV are shown.

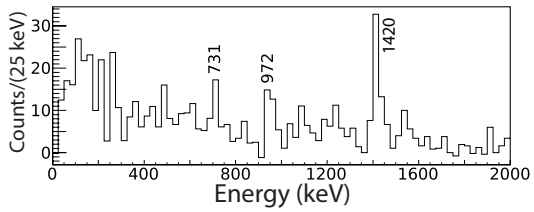

FIG. 19: Background-subtracted $\gamma\gamma$ coincidence spectrum for ^{41}P, gated on the 172(1)-keV transition. Statistics for the other transitions are insufficient for coincidence analysis.

TABLE V: Energy levels and associated γ-ray transitions observed in ^{41}P. Branching ratios and relative intensities of all transitions are also given.

E_{level} [keV]	J^π	τ (ps)	E_γ [keV]	Branching	Intensity
172(1)	$(3/2^+)$	652(55)	172(1)	100	100(2.3)
1148(4)	$(5/2^+)$	-	972(4)	100(14)	4.4(0.6)
			1148(4)	70(14)	3.1(0.6)
1592(4)	-	-	1420(4)	100	12.1(1.1)
2323(5)	-	-	731(2)	100	3.9(0.6)
-	-	-	443(2)	-	1.6(0.4)
-	-	-	1405(5)	-	12.3(1.1)

than 2% [32]. Based on the observed intensities of the 443(2) and 1420(4) keV transitions, a branching ratio of 12(3)% is deduced if they decay from the same state. Without sufficient evidence to place the 443(2)-keV transition anywhere else, it is suggested that it be removed from its current placement and be considered unplaced. It was also not possible to place the newly observed transition at 1405(5) keV in the level scheme.

The properties of the 172(1) and 1148(4)-keV levels are consistent with the predicted $3/2^+_1$ and $5/2^+_1$ states, as indicated by previous works [6, 32]. The 1592(4)-keV level most likely corresponds either to the predicted $5/2^+_3$ or $7/2^+_1$ state.

A very pronounced lifetime effect is visible for the 172(1)-keV transition that yields a mean lifetime of 652(55) ps. This is an order of magnitude longer than the shell-model prediction of 41 ps, but the calculated energy of the level, at 274 keV, is substantially greater than the measured value. Our lifetime measurement is consistent within uncertainty with the previous measurement of 550(70) ps by Riley *et al.* [45].

The shell-model calculations predict that the 172(1)-keV transition is nearly pure $M1$, with a mixing ratio of -0.07. Using this value yields $B(M1; (3/2^+) \rightarrow (1/2^+)) = 0.017(2)\ \mu_N^2$. The SDPF-MU shell-model calculations predict a $B(M1; 3/2^+_1 \rightarrow 1/2^+_1)$ value of 0.055 μ_N^2, a factor of three larger than observed.

F. ^{42}P

No previous spectroscopy of ^{42}P has been reported. Figure 20 shows the fitted, Doppler-reconstructed γ-ray spectrum taken in coincidence with the ^{42}P reaction residues. Eight γ-ray transitions are reported for the first time. Due to low statistics, a coincidence analysis was not possible and none of these transitions could be placed within a level scheme. The transition energies and their relative intensities are reported in Table VI. The predicted level scheme for ^{42}P is shown in Fig. 21 for completeness.

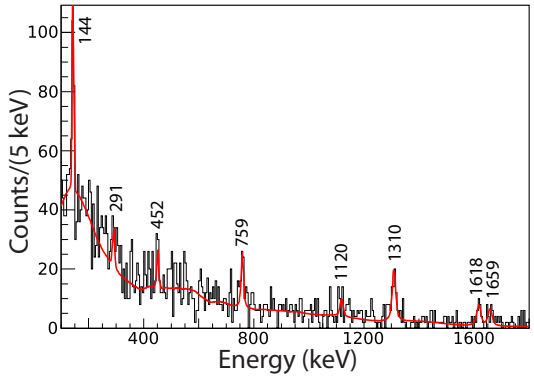

FIG. 20: Doppler-corrected (v/c = 0.325) γ-ray spectrum taken with GRETINA in coincidence with ^{42}P as identified with the S800 spectrograph. The red curves represent the GEANT4 fit to the data.

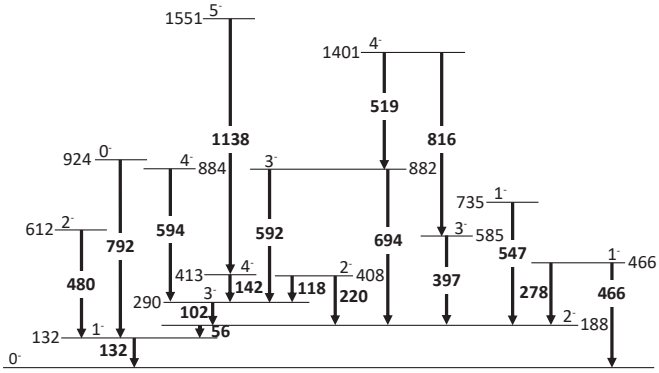

FIG. 21: Predicted ^{42}P level scheme based on the SDPF-MU shell-model calculation. All predicted levels below 2 MeV are shown.

TABLE VI: Observed γ-ray transitions in ^{42}P and their relative intensities.

E_γ [keV]	Intensity
144(1)	100(12)
291(2)	12(4)
452(2)	15(5)
759(3)	35(7)
1120(7)	18(6)
1310(3)	64(9)
1618(4)	33(7)
1659(8)	28(6)

G. Discussion of quadrupole collective structures

Before large-basis configuration interaction (CI) calculations were possible, the Nilsson model, for a selected axial deformation, provided a qualitative interpretation of the spectra and electromagnetic transitions for a variety of nuclei. While the SDPF-MU shell-model calculations in the available configuration space capture the structure and collectivity well for the neutron-rich P isotopes, for heavier nuclei where the CI basis dimensions becomes large, the Nilsson model may still be one of the few viable options to interpret collective structures observed in experiments. Thus, it is useful, for our case of medium mass neutron-rich nuclei, to examine to what extent the full CI calculation results for complex odd-even and odd-odd nuclei can be understood in terms of the Nilsson scheme.

Close to the N = 20 shell gap, ^{37}P is remarkably well described by the SDPF-MU shell-model calculations and displays an excitation scheme without collective features. For the more neutron-rich isotopes ^{39,41}P, it is worthwhile to examine the quadrupole-collective structures predicted by the shell-model calculations. Figure 22 shows the $E2$ map for ^{39,41}P. The networks show for each (positive-parity) state J a dot with a radius that scales with the magnitude of the spectroscopic quadrupole moment and where the color indicates the sign of the quadrupole moment (blue: negative; red: positive). The lines connecting the states indicate $E2$ transitions and the line thickness scales with the magnitude of the transition matrix element $M(E2)$. For the low-lying states, band-like structures emerge. For prolate deformations, the lowest proton Nilsson orbitals $[N, n_z, \Lambda]\Omega^\pi$ just above Z = 14 are (a) $[211]1/2^+$ (for $\beta \leq 0.3$) and (b) $[202]5/2^+$ (for $\beta \geq 0.3$). For ^{39}P and ^{41}P, the bands that start with $1/2^+$ could be associated with Nilsson state (a). The pattern for the higher-energy states is more complex. In ^{39}P there is some indication of a $5/2^+$ that could be associated with Nilsson state (b). The large positive quadrupole moments could indicate states that form band heads built on three quasiparticle states, but definitive associations with the Nilsson model are not possible.

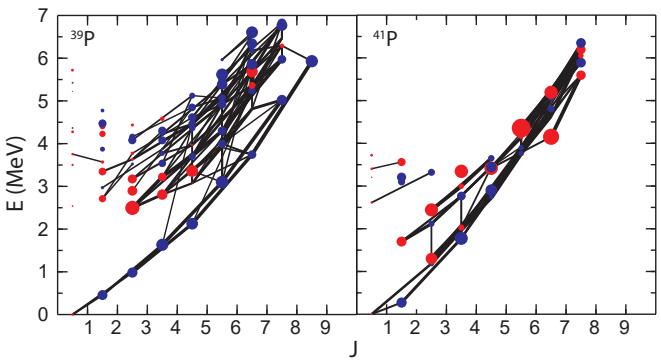

FIG. 22: $E2$ map for ^{39,41}P. The networks show for each (positive-parity) state J a dot with a radius that scales with the magnitude of the spectroscopic quadrupole moment and where the color indicates the sign of Q (blue: negative; red: positive). The lines connecting the states indicate $E2$ transitions and their thickness scales with the magnitude of the connecting transition matrix element $M(E2)$.

Figure 23 shows the $E2$ maps for ^{38,40,42}P. For prolate deformations, the neutron negative-parity Nilsson orbitals are (c) $[321]3/2^-$ for $N = 22$ and (d) $[312]5/2^-$ for $N = 24$. Thus for ^{38}P one may look for bands from the two-quasiparticle state (a, c) with $K^\pi = 1^-$ and 2^-. The lowest band starting at $J^\pi = 1^-$ might be associated with the $K^\pi = 1^-$ band. For ^{40}P one may expect bands from the two-quasiparticle state (a, d) with $K^\pi = 2^-$ and 3^-. Indeed, the lowest set of states strongly connected by $E2$ matrix elements starts at $J^\pi = 2^-$. For both nuclei, the higher-lying band structures are too complex to be easily associated with simple deformed configurations. The corresponding $E2$ network for ^{42}P has lost all simplicity but displays positive Q moments, signaling oblate deformation, similar to ^{42}Si.

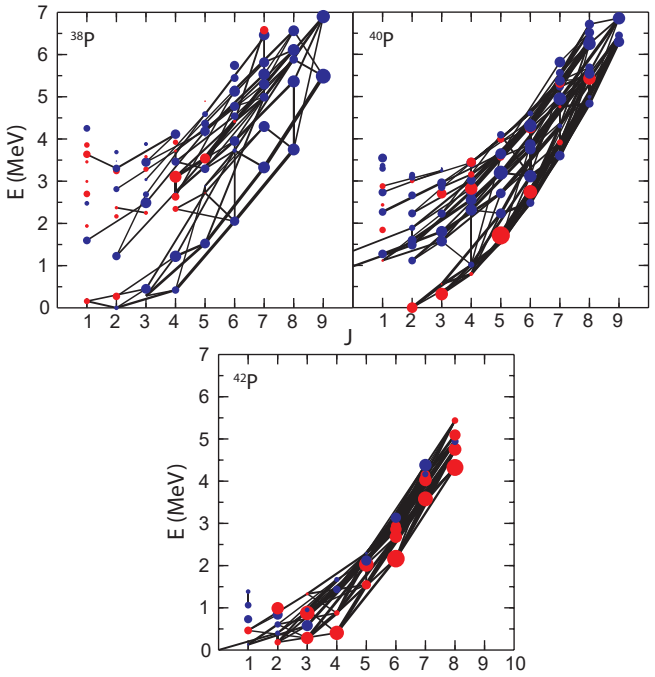

FIG. 23: Same as Fig. 22 but for the even-A ^{38,40,42}P.

IV. SUMMARY

The in-beam γ-ray spectroscopy of neutron-rich phosphorus isotopes produced by fragmentation of a ^{45}Cl projectile beam on a ^{12}C target is reported. Fifteen, 20, 16, 8, 1, and 8 new transitions were observed for ^{37}P, ^{38}P, ^{39}P, ^{40}P, ^{41}P, and ^{42}P, respectively. $\gamma\gamma$ coincidence relationships were used to inform the placement of the γ-ray transitions into level schemes. The level schemes, particularly for the even-N isotopes, show a remarkably good agreement with SDPF-MU shell-model calculations, allowing tentative spin-parity assignments to be proposed for many of the low-lying levels, and confirming that this shell-model effective interaction optimized for Si and S isotopes captures the nuclear structure of the $Z = 15$ isotopes as well. For the complex level structure of ^{40}P, spin-parity assignments from comparison to the shell-model calculations were not possible due to the high level density; thus more experimental information is needed to characterize the reported levels. Excited-state lifetimes in the hundreds of picoseconds to nanosecond range were obtained for levels in ^{38}P and ^{41}P from γ-ray lineshape analyses aided by GEANT4 simulations. From an analysis of the $E2$ transition matrix elements and moments calculated within the shell model, simple Nilsson configurations are suggested for the low-lying states in ^{38,39,40,41}P. The variety of shapes and occurrence of quadrupole collective structures may make the neutron-rich P isotopes interesting cases for sub-barrier Coulomb excitation measurements to probe the predicted evolution in shape and collectivity as $N = 28$ is approached.

Acknowledgments

This work was supported by the U.S. National Science Foundation (NSF) under Grant No. PHY-1565546, by the DOE National Nuclear Security Administration through the Nuclear Science and Security Consortium, under Award No. DE-NA0003180, and by the U.S. Department of Energy, Office of Science, Office of Nuclear Physics, under Grants No. DE-SC0020451. GRETINA was funded by the DOE Office of Science. Operation of the array at NSCL was supported by the DOE under Grant No. DE-SC0019034. B.A.B. acknowledges support from NSF Grant No. PHY-1811855.

[1] O. Sorlin and M.-G. Proquet, Prog. Part. Nucl. Phys. **61**, 602 (2008).
[2] O. Sorlin and M.-G. Porquet, Phys. Scr. T152, 014003 (2013).
[3] T. Otsuka, A. Gade, O. Sorlin, T. Suzuki, and Y. Utsuno, Rev. Mod. Phys. **92**, 015002 (2020).
[4] H. Scheit, T. Glasmacher, B. A. Brown, J. A. Brown, P. D. Cottle, P. G. Hansen, R. Harkewicz, M. Hellström, R. W. Ibbotson, J. K. Jewell, K. W. Kemper, D. J. Morrissey, M. Steiner, P. Thirolf, and M. Thoennessen, Phys. Rev. Lett. **77**, 3967 (1996).
[5] T. Glasmacher, B.A. Brown, M.J. Chromik, P.D. Cottle, M. Fauerbach, R.W. Ibbotson, K.W. Kemper, D.J. Morrissey, H. Scheit, D.W. Sklenicka, and M. Steiner, Phys.

Lett. **395**, 163 (1997).
[6] B. Bastin *et al.*, Phys. Rev. Lett. **99**, 022503 (2007).
[7] S. Takeuchi *et al.*, Phys. Rev. Lett. **109**, 182501 (2012).
[8] L. Gaudefroy, O. Sorlin, F. Nowacki, D. Beaumel, Y. Blumenfeld, Z. Dombrádi, S. Fortier, S. Franchoo, S. Grévy, F. Hammache, K. W. Kemper, K. L. Kratz, M. G. St. Laurent, S. M. Lukyanov, L. Nalpas, A. N. Ostrowski, Yu.-E. Penionzhkevich, E. C. Pollacco, P. Roussel, P. Roussel-Chomaz, D. Sohler, M. Stanoiu, and E. Tryggestad Phys. Rev. C **78**, 034307 (2008).
[9] L. Gaudefroy, O. Sorlin, D. Beaumel, Y. Blumenfeld, Z. Dombradi, S. Fortier, S. Franchoo, M. Gelin, J. Gibelin, S. Grevy, F. Hammache, F. Ibrahim, K. W. Kemper, K.-L. Kratz, S. M. Lukyanov, C. Monrozeau, L. Nalpas, F. Nowacki, A. N. Ostrowski, T. Otsuka, Yu.-E. Penionzhkevich, J. Piekarewicz, E. C. Pollacco, P. Rousset-Chomaz, E. Rich, J. A. Scarpaci, M. G. St. Laurent, D. Sohler, M. Stanoiu, T. Suzuki, E. Tryggestad, and D. Verney, Phys. Rev. Lett. **97**, 092501 (2006).
[10] M. Zielińska, A. Görgen, E. Clément, J. -P. Delaroche, M. Girod, W. Korten, A. Bürger, W. Catford, C. Dossat, J. Iwanicki, J. Libert, J. Ljungvall, P. J. Napiorkowski, A. Obertelli, D. Pietak, R. Rodríguez-Guzmán, G. Sletten, J. Srebrny, Ch. Theisen, and K. Wrzosek, Phys. Rev. C **80**, 014317 (2009).
[11] R. Winkler, A. Gade, T. Baugher, D. Bazin, B. A. Brown, T. Glasmacher, G. F. Grinyer, R. Meharchand, S. McDaniel, A. Ratkiewicz, and D. Weisshaar, Phys. Rev. Lett. **108**, 182501 (2012).
[12] E. Lunderberg, A. Gade, V. Bader, T. Baugher, D. Bazin, J. S. Berryman, B. A. Brown, D. J. Hartley, F. Recchia, S. R. Stroberg, D. Weisshaar, and K. Wimmer, Phys. Rev. C **94**, 064327 (2016).
[13] A. Gade, J. A. Tostevin, V. Bader, T. Baugher, D. Bazin, J. S. Berryman, B. A. Brown, C. Aa. Diget, T. Glasmacher, D. J. Hartley, E. Lunderberg, S. R. Stroberg, F. Recchia, A. Ratkiewicz, D. Weisshaar, and K. Wimmer, Phys. Rev. C **93**, 054315 (2016).
[14] S. R. Stroberg, A. Gade, J. A. Tostevin, V. M. Bader, T. Baugher, D. Bazin, J. S. Berryman, B. A. Brown, C. M. Campbell, K. W. Kemper, C. Langer, E. Lunderberg, A. Lemasson, S. Noji, F. Recchia, C. Walz, D. Weisshaar, and S. J. Williams, Phys. Rev. C **90**, 034301 (2014).
[15] S. R. Stroberg, A. Gade, J. A. Tostevin, V. M. Bader, T. Baugher, D. Bazin, J. S. Berryman, B. A. Brown, C. M. Campbell, K. W. Kemper, C. Langer, E. Lunderberg, A. Lemasson, S. Noji, T. Otsuka, F. Recchia, C. Walz, D. Weisshaar, and S. Williams, Phys. Rev. C **91**, 041302(R) (2015).
[16] L. Gaudefroy, Phys. Rev. C **81**, 064329 (2010).
[17] Y. Utsuno, T. Otsuka, B.A. Brown, M. Honma, T. Mizusaki, and N. Shimizu, Phys. Rev. C **86**, 051301 (2012).
[18] Y. Utsuno, N.Shimizu, T. Otsuka, T. Yoshida, Y. Tsunoda, Phys. Rev. Lett. **114**, 032501 (2015).
[19] J. J. Parker, IV, I. Wiedenhöver, P.D. Cottle, J. Baker, D. McPherson, M.A. Riley, D. Santiago-Gonzalez, A. Volya, V.M. Bader, T. Baugher, D. Bazin, A. Gade, T. Ginter, H. Iwasaki, C. Loelius, C. Morse, F. Recchia, D. Smalley, S.R. Stroberg, K. Whitmore, D. Weisshaar, A. Lemasson, H.L. Crawford, A.O. Macchiavelli, and K. Wimmer, Phys. Rev. Lett. **118**, 052501 (2017)
[20] D. Santiago-Gonzalez, I. Wiedenhöver, V. Abramkina, M. L. Avila, T. Baugher, D. Bazin, B. A. Brown, P. D. Cottle, A. Gade, T. Glasmacher, K. W. Kemper, S. McDaniel, A. Rojas, A. Ratkiewicz, R. Meharchand, E. C. Simpson, J. A. Tostevin, A. Volya, and D. Weisshaar, Phys. Rev. C **83**, 061305(R) (2011).
[21] S. R. Stroberg, A. Gade, T. Baugher, D. Bazin, B. A. Brown, J. M. Cook, T. Glasmacher, G. F. Grinyer, S. McDaniel, A. Ratkiewicz, and D. Weisshaar Phys. Rev. C **86**, 024321 (2012)
[22] B. Longfellow, D. Weisshaar, A. Gade, B. A. Brown, D. Bazin, W. W. Brown, B. Elman, J. Pereira, D. Rhodes, and M. Spieker, Phys. Rev. Lett. **125**, 232501 (2020).
[23] A. Gade and S. N. Liddick, J. Phys. G **43**, 024001 (2016).
[24] F. Rotaru, F. Negoita, S. Grévy, J. Mrazek, S. Lukyanov, F. Nowacki, A. Poves, O. Sorlin, C. Borcea, R. Borcea, A. Buta, L. Cáceres, S. Calinescu, R. Chevrier, Zs. Dombrádi, J. M. Daugas, D. Lebhertz, Y. Penionzhkevich, C. Petrone, D. Sohler, M. Stanoiu, and J. C. Thomas, Phys. Rev. Lett. **109**, 092503 (2012).
[25] C. Force, S. Grevy, L. Gaudefroy, O. Sorlin, L. Caceres, F. Rotaru, J. Mrazek, N. L. Achouri, J. C. Angelique, F. Azaiez, B. Bastin, R. Borcea, A. Buta, J. M. Daugas, Z. Dlouhy, Zs. Dombradi, F. De Oliveira, F. Negoita, Y. Penionzhkevich, M. G. Saint-Laurent, D. Sohler, M. Stanoiu, I. Stefan, C. Stodel, and F. Nowacki, Phys. Rev. Lett. **105**, 102501 (2010).
[26] R. W. Ibbotson, T. Glasmacher, P. F. Mantica, and H. Scheit, Phys. Rev. C **59**, 642 (1999).
[27] L. K. Fifield, R. Chapman, J. L. Durell, J. N. Mo, R. J. Smith, P. J. Woods, B. R. Fulton, R. A. Cunningham, P. V. Drumm, Nucl. Phys. A **484**, 117 (1988).
[28] A. Hodsdon, R. Chapman, X. Liang, F. Haas, J. Ollier, E. Caurier, F. Nowacki, M.-D. Salsac, F. Azaiez, S. Beghini, B. Behera, M. Burns, L. Corradi, D. Curien, A. N. Deacon, Zs. Dombrádi E. Farnea, E. Fioretto, A. Gadea, A. Jungclaus, K. L. Keyes, A. Latina, N. Mărginean, G. Montagnoli, D. Napoli, D. O'Donnell, A. Papenberg, F. Scarlassara, J. F. Smith, K.-M. Spohr, M. Stanoiu, A. Stefanini, S. Szilner, M. Trotta, C. Ur, D. Verney, and Z. Wang, Phys. Rev. C **75**, 034313 (2007).
[29] Vandana Tripathi, R. S. Lubna, B. Abromeit, H. L. Crawford, S. N. Liddick, Y. Utsuno, P. C. Bender, B. P. Crider, R. Dungan, P. Fallon, K. Kravvaris, N. Larson, A. O. Macchiavelli, T. Otsuka, C. J. Prokop, A. L. Richard, N. Shimizu, s. L. Tabor, A. Volya, and S. Yoshiba, Phys. Rev. C **95**, 024308 (2017).
[30] R. Chapman *et al.*, Phys. Rev. C **92**, 044308 (2015).
[31] O. Sorlin, Zs. Dombrádi, D. Sohler, F. Azaiez, J. Timár, Yu. -E. Penionzhkevich, F. Amorini, D. Baidorodin, A. Bauchet, F. Becker, M. Belleguic, C. Borcea, C. Bourgeois, Z. Dlouhy, C. Donzaud, J. Duprat, L. Gaudefroy, D. Guillemaud-Mueller, F. Ibrahim, M. J. Lopez, R. Lucas, S. M. Lukyanov, V. Maslov, J. Mrazek, C. Moore, F. Nowacki, F. Pougheon, M. G. Saint-Laurent, F. Sarazin, J. A. Scarpaci, G. Sletten, M. Stanoiu, C. Stodel, M. Taylor, and Ch. Theisen, Eur. Phys. J. A **22**, 173 (2004).
[32] L. A. Riley, D. Bazin, J. Belarge, P. C. Bender, B. A. Brown, P. D. Cottle, B. Elman, A. Gade, S. D. Gregory, E. B. Haldeman, K. W. Kemper, B. R. Klybor, M. A. Liggett, S. Lipschutz, B. Longfellow, E. Lunderberg, T. Mijatovic, J. Pereira, L. M. Skiles, R. Titus, A. Volya, D. Weisshaar, J. C. Zamora, and R. G. T. Zegers, Phys. Rev. C **100**, 044312 (2019); Erratum Phys. Rev. C **101**, 059902 (2020).
[33] A. Gade and B. M. Sherrill, Phys. Scrip. **91**, 053003

(2016).
[34] D. J. Morrissey, B.M. Sherrill, M. Steiner, A. Stolz, and I. Wiedenhoever, Nucl. Instrum. Methods Phys. Res., Sect. **B 204**, 90 (2003).
[35] D. Bazin, J. A. Caggiano, B. M. Sherrill, J. Yurkon, and A. Zeller, Nucl. Instrum. Methods in Phys. Res., Sect. **B 204**, 629 (2003).
[36] J. Yurkon, D. Bazin, W. Benenson, D. J. Morrissey, B. M. Sherrill, D. Swan, and R. Swanson, Nucl. Instrum. Methods Phys. Res., Sect. A 422, 291 (1999).
[37] S.Paschalis, I. Y. Lee, A. O. Macchiavelli, C. M. Campbell, M. Cromaz, S. Gros, J. Pavan, J. Qian, R. M. Clark, H. L. Crawford, D. Doering, P. Fallon, C. Lionberger, T. Loew, M. Petri, T. Stezelberger, S. Zimmerman, D. C. Radford, K. Lagergren, D. Weisshaaaar, R. Winkler, T. Glasmacher, J. T. Anderson, and C. W. Beausang, Nucl. Instrum. Methods Phys. Res., Sect. **A 709**, 44 (2013).
[38] N. Nica, J. Cameron, B. Singh, *Nucl. Data Sheets* **113**, 1 (2012).
[39] J. Chen, *Nucl. Data Sheets* **152**, 1 (2018).
[40] J. Chen, *Nucl. Data Sheets* **140**, 1 (2017).
[41] D. Weisshaar, D. Bazin, P. C. Bender, C. M. Campbell, F. Recchia, V. Bader, T. Baugher, J. Belarge, M. P. Carpenter, H. L. Crawford, M. Cromaz, B. Elman, P. Fallon, A. Forney, A. Gade, J. Harker, N. Kobayashi, C. Langer, T. Lauritsen, I. Y. Lee, A. Lemasson, B. Longfellow, E. Lunderberg, A. O. Macchiavelli, K. Miki, S. Momiyama, S. Noji, D. C. Radford, M. Scott, J. Sethi, S. R. Stroberg, C. Sullivan, R. Titus, A. Wiens, S. Williams, K. Wimmer, S. Zhu, Nucl. Instrum. Methods in Phys. Res., Sect. **A 847**, 187 (2017).
[42] S. Agostinelli, J. Allison, K. Amako, J. Apostolakis, H. Araujo, P., M. Asai, D. Axen, S. Banerjee, G. Barrand, F. Behner, L. Bellagamba, J. Boudreau, L. Broglia, A. Brunengo, H. Burkhardt, S. Chauvie, J. Chuma, R. Chytracek, G. Cooperman, G. Cosmo, P. Degtyarenko, A. Dell'Acqua, G. Depaola, D. Dietrich, R. Enami, A. Feliciello, C. Ferguson, H. Fesefeldt, G. Folger, F. Foppiano, A. Forti, S. Garelli, S. Giani, R. Giannitrapani, D. Gibin, J.J. Gómez Cadenas, I. González, G. Gracia Abril, G. Greeniaus, W. Greiner, V. Grichine, A. Grossheim and S. Guatelli and P. Gumplinger and R. Hamatsu and K. Hashimoto and H. Hasui and A. Heikkinen and A. Howard and V. Ivanchenko and A. Johnson and F.W. Jones and J. Kallenbach and N. Kanaya and M. Kawabata and Y. Kawabata and M. Kawaguti, S. Kelner, P. Kent, A. Kimura, T. Kodama, R. Kokoulin, M. Kossov, H. Kurashige, E. Lamanna, T. Lampén, V. Lara, V. Lefebure, F. Lei, M. Liendl, W. Lockman, F. Longo, S. Magni, M. Maire, E. Medernach, K. Minamimoto, P. Mora de Freitas, Y. Morita, K. Murakami, M. Nagamatu, R. Nartallo, P. Nieminen, T. Nishimura, K. Ohtsubo, M. Okamura, S. O'Neale, Y. Oohata, K. Paech, J. Perl, A. Pfeiffer, M.G. Pia, F. Ranjard, A. Rybin, S. Sadilov, E. Di Salvo, G. Santin, T. Sasaki, N. Savvas, Y. Sawada, S. Scherer, S. Sei, V. Sirotenko, D. Smith, N. Starkov, H. Stoecker, J. Sulkimo, M. Takahata, S. Tanaka, E. Tcherniaev, E. Safai Tehrani, M. Tropeano, P. Truscott, H. Uno, L. Urban, P. Urban, M. Verderi, A. Walkden, W. Wander, H. Weber, J.P. Wellisch, T. Wenaus, D.C. Williams, D. Wright, T. Yamada, H. Yoshida, and D. Zschiesche, Nucl. Instrum. Methods Phys. Res., Sect. **A 506**, 250 (2003).
[43] L.A. Riley, D. Weisshaar, H.L. Crawford, M.L. Agiorgousis, C.M. Campbell, M. Cromaz, P. Fallon, A. Gade, S.D. Gregory, E.B. Haldeman, L.R. Jarvis, E.D. Lawson-John, B. Roberts, B.V. Sadler, C.G. Stine, Nucl. Instrum. Methods Phys. Res., Sect **A 1003**, 165305 (2021).
[44] NuShellX, http://www.garsington.eclipse.co.uk/
[45] L. A. Riley, D. Bazin, J. Belarge, P. C. Bender, B. A. Brown, P. D. Cottle, B. Elman, A. Gade, S. D. Gregory, E. B. Haldeman, K. W. Kemper, B. R. Klybor, M. A. Liggett, S. Lipschutz, B. Longfellow, E. Lunderberg, T. Mijatovic, J. Pereira, L. M. Skiles, R. Titus, A. Volya, D. Weisshaar, J. C. Zamora, and R. G. T. Zegers, Phys. Rev. C **101**, 059902 (2020).